RSC Advances

ROYAL SOCIETY OF CHEMISTRY

www.rsc.org/advances

Journal Name

ARTICLE

Ideal rear contact formed via employing a conjugated polymer for Si/PEDOT:PSS hybrid solar cells

Received 00th January 20xx,
Accepted 00th January 20xx

DOI: 10.1039/x0xx00000x

www.rsc.org/

Jiang Sheng, Dan Wang, Sudong Wu, Xi Yang, Li Ding, Juye Zhu, Junfeng Fang, Pingqi Gao and Jichun Ye*

Recently, Si/organic polymer hybrid solar cells are widely studied as the candidate of low-cost photovoltaics due to the simple low-temperature fabrication process. However, the rear electrode typically formed by directly depositing Al on the n-type Si is a Schottky contact, severely impacting the electron collecting efficiency. Here, an alcohol soluble polymer, poly[(9,9-bis(3'-(N, N-diethylamino)propyl)-2,7-fluorene)-alt-2,7-(9,9-dioctylfluorene)] (PFN), is firstly introduced to the Al/n-Si interface to improve the contact property, resulting in a remarkable reduced work function (WF) of Al electrode and thus a good Ohmic contact. An excellent photovoltaic efficiency of 13.35% is achieved in a planar device with a PFN layer. The facilitated electron collection efficiency associated with the Ohmic contact not only improves the fill factor, but also enhances the short circuit current. Furthermore, the open circuit voltage increases significantly mainly due to the constructive effect of the built-in electric field of the rear contact on the total built-in electric field of solar cell. Dark current-voltage, capacitance-voltage and electrochemical impedance spectra are used to systemically investigate the influence of PFN layer on the performance, with prospects to receiving high efficiency device with the quality rear contact.

1. Introduction

The inorganic/organic hybrid solar cells have attracted considerable research attention because of the advantages in solution process, low temperature, low cost fabrication and mechanical flexibility.[1] The breakthroughs in materials and device architecture are the key elements for the development of high performance solar cells. Up to now, the power conversion efficiency (PCE) of Si/PEDOT:PSS hybrid solar cell has been improved to 15% through the interface modification and material improvement.[2-4] The electrode, as a crucial part in this hybrid solar cell, collects the photo-generated charges to external circuit. Usually, the Al,[5, 6] Ti/Pd/Ag,[7] Ti/Ag[8] and In:Ga[9] are used to be deposited on the rear side of c-Si wafer as the electrode. Ideally, Ohmic contacts to semiconductors are typically constructed by depositing metal films with a chosen composition if the metal WFs are smaller than that of n-type semiconductor or larger than that of p-type semiconductor.[10] In the Si/PEDOT:PSS hybrid solar cells, the high WF metals, such as Al or Ag, are normally applied directly on the rear side of n-type Si wafer without high temperature annealing, which resulted in a Schottky contact with a high barrier height. This Schottky barrier not only reduces the electron collection efficiency, but also reversely decreases the total built-in electric field of hybrid solar cell, leading to an increased series resistance, a dropped short circuit current (J_{sc}) and deteriorated open circuit voltage (V_{oc}).

Reduction of the cathode WF through the surface modification at the cathode interfaces is an efficient way to form the Ohmic contacts.[11, 12] Low WF metals (e.g., Ca or Mg) are frequently used to facilitate electron injection.[13] However, these active metals are very sensitive to moisture and oxygen to seriously affect the device lifetime. Additionally, alkali metal salts (e.g., LiF and CsF) are also utilized to modify the interface of rear electrode.[13] Due to the insulation nature, the thicknesses of the alkaline metal salts should be controlled carefully to ensure a sufficient electron tunnelling. From another aspect, these films are deposited in the vacuum, which makes device fabrication more complicated. Solution process using the water/alcohol soluble conjugated polymers has been developed to modify the interface in polymer light emitting devices and polymer solar cells.[11, 13, 14] For these conjugated polymers, the conjugated backbone endows good conductivity and the surfactant-like side chains render good solubility of polymers in alcohol solvents. In addition, these polymers can reduce the WF of metal electrodes via strong interface dipoles, leading to an improved contact quality for the enhanced electron collection efficiency.

Ningbo Institute of Material Technology and Engineering, Chinese Academy of Sciences, Ningbo 315201, People's Republic of China. E-mail: jichun.ye@nimte.ac.cn

Electronic Supplementary Information (ESI) available: the details of PFN synthesis, the surface morphology of the PFN layer (Fig. S1), the details and pattern of TLM measurement (Fig. S2), the J-V curves of two Al electrode (Fig. S3) and the photovoltaic performance of hybrid solar cells with various PFN thickness (Fig. S4). See DOI: 10.1039/x0xx00000x

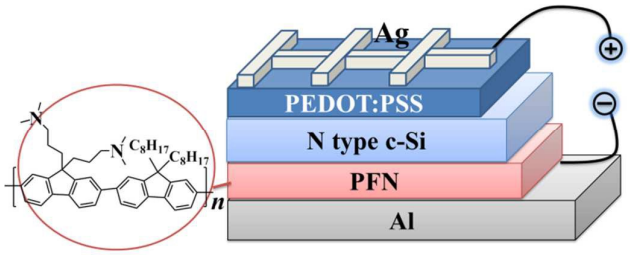

Fig. 1 Schematic drawing of PFN as the cathode interfacial layer in the Si/PEDOT:PSS hybrid solar cells.

Here, the PFN is incorporated into the cathode to reduce the WF of Al electrode for high electron collection efficiency in Si/PEDOT:PSS hybrid solar cells. PFN tunes down the Al WF value to be 3.62 eV from the original 4.31 eV, so that the Al/Si contact becomes an Ohmic contact from the previous Schottky contact. The interface dipoles create a reverse built-in electric field at the Al/PFN/Si interface to enhance the total built-in electric field to improve V_{oc}. The surface WF and current (capacitance)-voltage characteristics are presented to explain the effects on the photovoltaic properties of hybrid solar cells. A significant efficiency improvement is demonstrated from 10.28% for the solar cell without PFN modification to 13.35% for the solar cell with a PFN interlayer.

2. Experimental section

2.1 Preparation of PFN solution

All reagents were obtained from Sigma-Aldrich and Sinopharm Chemial Reagent Co, and used as received. All the used solvents were further purified before use. The PFN was synthesized by a process described in the previous literatures,[15-17] while the details were presented in Supporting Information. This interlayer material was dissolved in the methanol solution including a small amount of acetic acid (2 μl•ml^{-1}) to form a 2 mg•ml^{-1} PFN solution.

2.2 Fabrication of hybrid solar cells

One-side polished, n-type (100) float zone (FZ) Si wafers (resistivity, 1-5 Ω•cm) with the thickness of 300±15 μm were cut into 20×20 mm^2 squares as the substrates. Firstly, these substrates were cleaned sequentially in acetone, ethanol and deionized water, respectively. Then they were immersed in a solution including H_2SO_4 (98%) and H_2O_2 (30%) in the volume ratio of 1:3 at 100 °C for 15 min to remove any possible organic residues. Again, they were placed in a solution consisted of HCl (37%), H_2O_2 (30 %) and DI water in the volume ratio of 1:1:8 at 80 °C for 15 min to remove metallic residues. Finally, the wafers were immersed in diluted HF (5%) solution for 3 min to remove the native oxide, receiving H-terminated surfaces. The PFN solution was spin-coated on the rear side of wafer at a spin speed of 1000 rpm and then dried in the air, without any cross-linking treatment. Subsequently, the Al rear electrode with the thickness of 150 nm, was deposited by a vacuum thermal evaporation on the top of PFN layer. After exposing to ambient atmosphere for 1 h, the high conductive PEDOT:PSS (Clevios PH1000) solution mixed with the ethylene glycol (EG, 7 wt%) and Zonyl fulorosurfactant (0.1 wt%) was spin-coated on the front side of Si substrate at a speed of 1200 rpm and then thermally treated at 140 °C for 10 min to form a p-type emitter. A silver grid was finally deposited by thermal evaporation on PEDOT:PSS film surface using a shadow mask to complete the fabrication of the device. The device structure is illustrated in Fig. 1. The hybrid solar cell with the PFN modification was labelled as the PFN solar cell, and the hybrid solar cell without PFN was labelled as a reference solar cell.

2.3 Characterization

The ^{1}H and ^{13}C NMR spectra of PFN were collected by a Bruker AVANCE III spectrometer in deuterated chloroform solution operating respectively at 500 MHz (for ^{1}H) and 100 MHz (for ^{13}C), with tetramethylsilane as reference. Number-average (M_n) and weight-average (M_w) molecular weights were determined by a Waters GPC 2410 in tetrahydrofuran (THF) using a calibration curve of polystyrene standards. The thickness of PFN layer was measured by a spectroscopic ellipsometry (Uvisel, Horiba). The surface topography and scanning Kelvin probe microscopy (SKPM) of silicon wafers modified by PFN were observed by atomic force microscopy (AFM) in a Digital Instruments Dimension 3100 Nanoscope IV. The WF of Al film was measured by the ultraviolet photoelectron spectroscopy (UPS, Kratos AXIS Ultra DLD). The typical transmission line model (TLM) method was used to measure the contact resistance of the cathode interface between Al grid and n-type silicon (with PFN and without PFN). The resistance was determined by the current-voltage (*I-V*) curves between two contacts, measured by a Semiconductor parameter analyzer (Keithley 4200-SCS, USA). The minority carrier lifetimes of wafers were characterized by a microwave photoconductance decay (μ-PCD) technique (WT2000PVN, Semilab). The current density-voltage (*J-V*) characteristics of the solar cells were recorded with a Keithley 2400 digital source meter (Keithley, USA) under a simulated sunlight (100 mW/cm^2) illumination provided by a xenon lamp (Oriel, USA) with an AM 1.5 filter. The irradiation intensity was calibrated by a standard silicon photovoltaic device (Oriel, model 91150V). The cells were shielded by the opaque mask with an aperture area of 0.5×0.5 cm^2, with the shading area (11%) of Ag grids. And the temperature was actively controlled at 25 ± 0.5 °C during the measurements. The current capacitance-voltage (*C-V*) curve of hybrid solar cells was measured by a Keithley 4200-SCS Parameter Analyzer at a signal frequency of 1 KHz. The external quantum efficiency (EQE) system used a 300 W xenon light source with a spot size of 1×3 mm^2, calibrated with a silicon photodetector also from Newport. The electrochemical impedance spectra (EIS) were measured with an impedance analyzer (Solartron Analytical, 1260A) connected with a potentiostat (Solartron Analytical, 1287) under the dark condition. EIS spectra were recorded over the frequency range of 10^{-1}-10^6 Hz at room temperature.

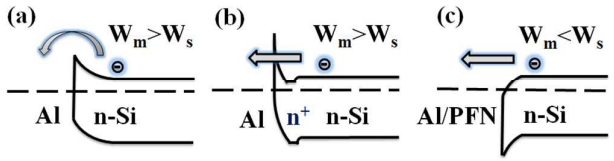

Fig. 2 Energy alignment of Al/ n-Si, Al/n^+-Si/n-Si and Al/PFN/ n-Si interfaces (W_m: metal WF; W_s: semiconductor WF). (a) When W_m>W_s, there is a Schottky barrier to retard the electron collection by the Al electrode. (b) After phosphorus diffusion, n^+ layer with heavy P-doped concentration narrows the depletion region at the interface and allows electrons to tunnel easily through the barrier, being an Ohmic contact. (c) After reducing the metal WF by interface modification, when W_m<W_s, Ohmic contact to n-Si is formed for the current flowing easily.

3 Results and discussion

3.1 Contact properties of rear electrode

In this study, the n-type wafers with the resistivity of 1-5 Ω•cm are used, which is equivalent to a phosphorous doping of 8.95×10^{14}-4.83×10^{15} cm^{-3} (low doping level). There are two conduction mechanisms, thermionic emission and field emission, for metal/semiconductor contacts as a function of the barrier height and width.[18, 19] With the low doping concentration, such as the n-Si in our study, the depletion region in the Schottky is wide and thus thermionic emission dominates, as illustrated in Fig. 2a. For such a case, the only way for the electrons to transfer to the Al electrode is to jump over the potential barrier by thermionic emission. According to the Schottky model, this barrier height (ϕ_b) can be predicted to be 0.26 eV, from the Equation 1:

$$\phi_b = \phi_m - \chi \quad (1)$$

where, the Al WF ϕ_m and the electron affinity χ are 4.31 eV[20202020] and 4.05 eV, respectively.[20] This Schottky barrier retards the electron collection at the rear electrode. Also, a built-in electric field is formed at the Al/n-Si interface, which is in the opposite direction to the built-in electric field of Si/PEDOT:PSS heterojunction, so that there is a V_{oc} drop of solar cell. Field emission takes place when the depletion layer is sufficiently narrow for the electrons to tunnel through if the semiconductor is highly doped, as shown in Fig. 2b. In one of our previous studies, a phosphorus diffusion process was utilized to form a high doping n^+ layer to facilitate the electron collection.[21] However, this diffusion process is conducted at a high temperature (>800 °C) with toxic gas, which is contradictory to the intrinsic benefit of Si/PEDOT:PSS hetrojunction solar cells. As an alternative, if the Al WF will be reduced effectively to a level of smaller than WF of n-Si, the energy band edge bends downwards, the electrons can freely move from semiconductor to electrode and an Ohmic contact is thus formed, as shown in Fig. 2c. Here, PFN layer is inserted into the Al/n-Si interface, which significantly decreases the surface WF of Al electrode to reverse the Schottky barrier, due to the influence of PFN dipoles and lone pairs.[22] As a result, the built-in electric field is also reversed to be in the same direction of the built-in electric field of Si/PEDOT:PSS junction, and thus the total built-in electric field of the device is enhanced and the improved V_{oc} of hybrid solar cell is predicted.

In order to quantify the contact properties of Al/Si and Al/PFN/Si interfaces, the TLM is conducted to measure the contact resistance. The detailed TLM method is described in the Supporting Information. The measurement schematics of the TLM test pattern is shown in Fig. S2. Fig. 3a displays characteristic *I-V* curves of the different interface contacts. The *I-V* curve of Al/n-Si interface shows the typical behaviour of a Schottky contact. While the *I-V* curve of Al/PFN/Si interface exhibits a linear current-voltage relationship, which is an evidence of being an Ohmic contact. The contact resistivity is deduced to be $(5.10 \pm 1.20)\times10^{-2}$ Ω•cm^2, similar to the values (10^{-2}-10^{-3} Ω•cm^2) for the Ohmic contact with a heavy doping layer of phosphorous.[23] Therefore, the contact property at rear electrode is dramatically improved by the modification of the PFN layer.

The PFN film processed with a spin coating method covers fully on the substrate and the thickness is about 10 nm without the cross-linking treatment, measured by the spectroscopic ellipsometer. To investigate the functions of PFN interfacial layer, the UPS is used to analyse the WF change on the Al film with PFN modification. Fig. 3b displays the UPS spectra of binding energy from Al film with or without a PFN layer on the top. The WF values reduce from the original 4.29±0.02 eV to 3.62±0.02 eV when a PFN layer is applied. This 0.67 eV decrease in WF value of the PFN/Al is similar to the value reported in polymer solar cell when PFN is used, indicating that the cross-linking process do not affect the WF tuning of PFN on the electrode materials.[11, 24] With this 0.67 eV decrease, the PFN/Al WF is smaller than that of n-Si, and the barrier height is dropped from 0.26 eV to -0.41 eV, consistent with a reported value of -0.43 eV.[25] The corresponding energy band diagram is illustrated in Fig. 2c.

The WF change by PFN modification is further measured by SKPM under ambient conditions because of the good air stability of PFN polymer.[17, 26] The same conductive tip (PtIr alloy) was used to probe the sample during the entire measurement to ensure that the WF values of tip remain constant. The surface potential (V_{sp}) is deduced from Equation 2:

$$\Phi_s = \Phi_t - eV_{sp} \quad (2)$$

where Φ_t, Φ_s and e are the conductive tip WF, the specimen WF, and the elementary charge, respectively. A lower surface potential on the dark SKPM images correspond to a higher WF

Journal Name

ARTICLE

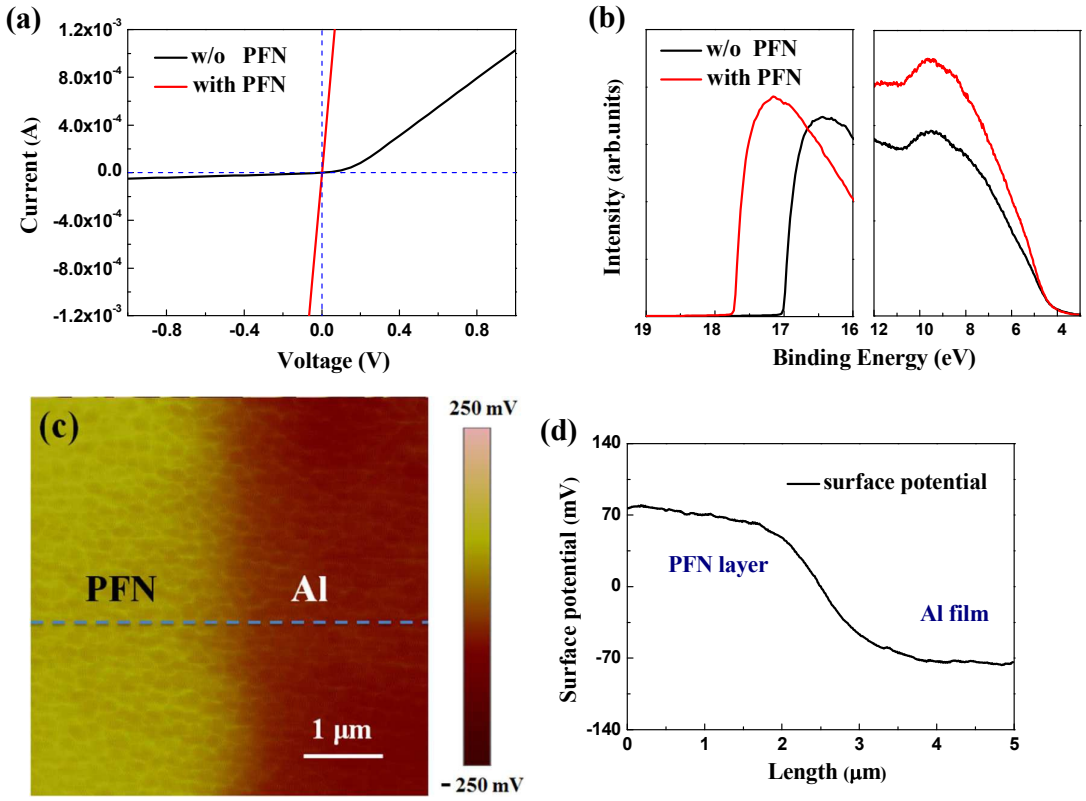

Fig. 3 (a) Current-voltage measurements between Al grids at the rear side of wafer with or without a PFN interfacial layer, (b) UPS spectra at high binding energy region (secondary electron cut-off) of Al film with or without a PFN layer on the top, (c) Surface potential images and (d) Cross-section profile of surface potential images along the dashed line by using SKPM to probe the surface potential difference of PFN and Al.

of the measured specimen.[4] From Fig. 3c, the surface potential of PFN/Al is much higher than the bare Al film, consistent with the UPS measurement. Fig. 3d displays the cross-section line profile of surface potential images, with a potential drop of about 145 mV by PFN modification.

3.2 Photovoltaic characteristics of hybrid solar cells

The devices of hybrid solar cells were fabricated to study the influence of PFN interlayer at the Al/Si interface on the photovoltaic performance. Firstly, the influence of various PFN thicknesses on the photovoltaic characteristics is investigated in Fig. S4 of Supporting Information. The *J-V* characteristics of devices are affected slightly by the thicknesses of PFN layer. Fig. 4a shows the *J-V* curves for the Si/PEDOT:PSS hybrid solar cells based on the rear electrode with or without a PFN interfacial layer, under a simulated sunlight (100 mW/cm^2) illumination. The photovoltaic properties are summarized in Table 1. The PFN solar cell displays an excellent photovoltaic performance, a high PCE of 13.35% with a V_{oc} of 0.582 V, a J_{sc} of 29.57 mA/cm^2 and a *FF* of 77.56%. This photovoltaic efficiency is improved significantly, representing a 30.05% increase from a 10.28% PCE in the reference solar cell. After inserting a PFN layer, the series resistance of device with the Ohmic contact is reduced from 10.85 Ω•cm^2 in the reference device to 7.37 Ω•cm^2. Furthermore, the J_{sc} value of PFN solar cell exhibits a 11.29% increase from 26.57 mA/cm^2 in the reference solar cell, because the electron collection efficiency of hybrid solar cell is enhanced by the improved contact quality at the rear electrode. It is worth noting that a significant V_{oc} increase (58 mV) is observed in the PFN device, from a value of 0.528 V in the reference device. As discussed in Section 3.1, when the PFN is inserted, the built-in electric field at the Al/Si interface is reversed to be in the same direction of the built-in electric field of Si/PEDOT:PSS junction,

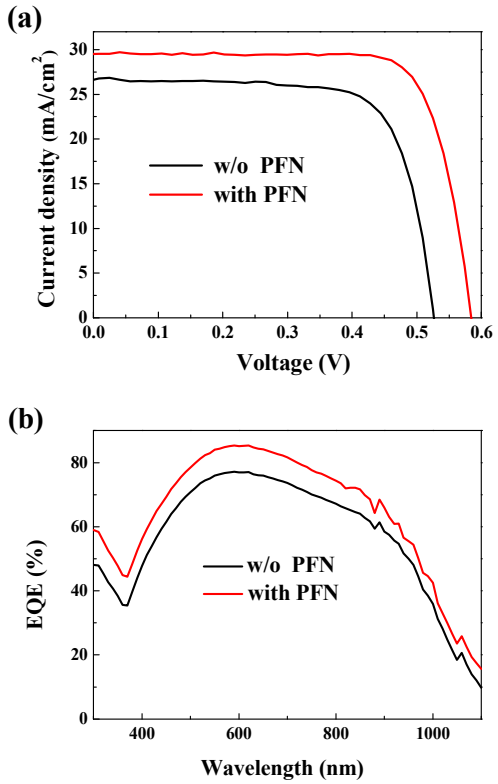

Fig. 4 (a) Current density *vs.* voltages curves under a simulated sunlight (100 mW/cm^2) illumination, (b) External quantum efficiencies of Si/PEDOT:PSS hybrid solar cells based on the rear electrode with or without a PFN interfacial layer.

and thus the V_{oc} of hybrid solar cell is improved. The improved V_{oc} could also come from the surface passivation effect of the PFN layer at the rear surface of n-Si, which will be further explored in Table S2 in Supporting Information. The PFN device exhibits a larger *FF* value as a result of smaller R_s and larger R_{sh}. As a conclusion, the significant PCE improvement in PFN device can be ascribed to the better contact quality and the enhanced total built-in electric field caused by the PFN dipoles. Fig. 4b shows the EQE curves of solar cells. The PFN device exhibits larger EQE values in the region of 300-1100 nm than that of reference device. For the PFN device, a calculated J_{sc} of 29.26 mA/cm^2 is confirmed by integrating the EQE curve, larger than 26.14 mA/cm^2 of the reference device. This calculated value proves the enhanced electron collection efficiency after PFN modification, in well accordance with the measured J_{sc} results. It is worth noting that the increase in EQE becomes smaller in the long wavelength region, which is likely caused by the reduced reflectivity of back surface after the insertion of the PFN layer.

3.3 Electric characteristics of hybrid solar cells

Table 1 Photovoltaic properties of the Si/PEDOT:PSS hybrid solar cells with Al/Si and Al/PFN/Si rear electrodes.

devices	J_{sc} (mA/cm^2)	V_{oc} (mV)	*FF* (%)	η (%)	R_s (Ω•cm^2)	R_{sh} (Ω•cm^2)
w/o PFN	26.57 ±0.52	524 ±5	73.87 ±0.43	10.28 ±0.47	10.85 ±0.62	8972 ±10
with PFN	29.57 ±0.46	582 ±5	77.56 ±0.38	13.35 ±0.31	7.37 ±0.54	17524 ±15

In order to further evaluate the electric properties of hybrid solar cells after inserting the PFN interlayer, the dark *J-V* and C-*V* characteristics are investigated systemically. Fig. 5a shows the dark *J-V* curves for the Si/PEDOT:PSS hybrid solar cells. Compared to the reference device, the dark current density of PFN device is remarkably smaller at forward bias voltages, indicating that the recombination of charge carriers is reduced significantly in the PFN device. The improved electron collection efficiency could reduce the probability of recombination at the rear surface. Additionally, the rear side of wafer is passivated by the PFN layer to some extent, showing slightly larger minority carrier lifetime in Table S2 of Supporting Information.

The diode ideality factor (*n*), the reversed saturation current density (J_s) and the barrier height (Φ_{bi}) are derived from the ln *J-V* curves (Fig. 5b) and summarized in Table 2, based on the Equations 3 and 4.[27] The dark *J-V* curves can be simulated according the diode equations, as follow:

$$J = J_s\left(\exp(\frac{eV}{nkT}) - 1\right) \quad (3)$$

$$J_s = A^* A T^2 \exp\left(-\frac{\Phi_{bi}}{kT}\right) \quad (4)$$

where *A* is the contact area, A^* is the effective Richardson constant (about 252 Acm^{-2}K^{-2} for n-type silicon), *T* is the absolute temperature (298 K), κ is the Boltzmann constant, and Φ_{bi} is the barrier height of devices. At the reverse bias voltages, the dark ln*J* values of PFN device are much larger than those of reference device, with better electron extraction at Al/PFN/Si electrode leading to higher electron collection efficiency under visible light illumination condition. This result concludes an agreement with the behaviour of organic light emitting diode and organic photovoltaic form the previous literatures.[11, 28] The *n* values of solar cells are obtained from fitting the slopes of tangent lines of ln*J-V* curves at the region of 0.3-0.6 V. The PFN solar cell presents better heterojunction quality of Si/PEDOT:PSS with a smaller *n* value and a higher J_s value, suggesting a drastic reduction in charge recombination in the Si/PEDOT:PSS heterojunction.

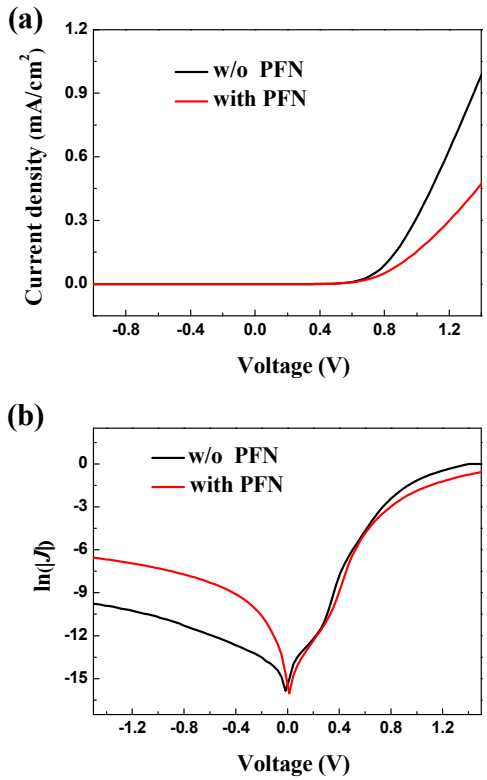

Fig. 5 (a) Dark current density *vs.* voltages curves and (b) ln*J vs.* voltages curves in the dark condition of the Si/PEDOT:PSS hybrid solar cells based on the rear electrodes with or without a PFN interfacial layer.

Also, the barrier height Φ_{bi} of PFN solar cell evidently increases to 0.899 eV from the 0.780 eV of the reference solar cell, because the total built-in electric field is enhanced once the contact barrier is reversed when PFN is applied. This favourable internal electric field leads to high separation efficiency of photo-generated charge carrier. However, the V_{oc} value is much lower than the Φ_{bi} value, due to the current leakage and carrier charge recombination at the various interfaces. Therefore, if the surfaces passivation is further improved, the PFN device will receive a larger V_{oc}, even approaching to values of 0.7 V for the traditional Si solar cells.[29]

Furthermore, the series resistance is also extracted from the forward dark *J-V* curve of solar cells, as shown in Fig. 6a, according to Equation 5:[30]

$$\frac{d(V)}{d(\ln J)} = R_{sd}AJ + \frac{nq}{\kappa T} \quad (5)$$

where R_{sd} is the series resistance of device under the dark condition, and q is the elementary charge. Fig. 6a clearly shows that the plot of PFN solar cell has smaller slope, compared to that of the reference device. and thus the R_{sd} value for the PFN device is much smaller, only half of that of the reference device, which is consistent with the R_s values derived when illuminated.

Table 2 Summaries of diode ideality factor (n), reversed saturation current density, barrier height (Φ_{bi}) and series resistance (R_{sd}) fitted from the dark ln*J*-V curve of Si/PEDOT:PSS hybrid solar cells based on the different rear electrodes.

devices	n	J_s (A/cm^2)	Φ_{bi} (eV)	R_{sd} (Ω•cm^2)
w/o PFN	2.45	5.74×10^{-7}	0.780	3.50
with PFN	1.46	7.65×10^{-9}	0.899	1.88

Both of the PFN device and reference device are evaluated by the *C-V* measurement to analysis the PFN influence on the built-in potential. Fig. 6b displays C^{-2}-*V* plots of hybrid solar cells and the value of V_{bi} can be deduced from the *x*-axis intercept of straight line of the C^{-2}-*V* curve, based on the Mott-Schottky relation:[31]

$$C^{-2} = \frac{2(V_{bi} - V)}{A^2 e\varepsilon\varepsilon_0 N_A} \quad (6)$$

where V_{bi} is the built-in potential, V is the applied voltage, ε is the relative dielectric constant, ε_0 is the permittivity of vacuum, and N_A the concentration of acceptor impurities. The V_{bi} value for PFN device is much larger than that of the reference device, agreed with the enhanced barrier height in the PFN device. From the dark *J-V* and C^{-2}-*V* results, it is worth noting that the PFN interface modification reverses the band bending, which remarkably enhances the total built-in electric field in hybrid solar cell, leading to a better heterojunction of Si/PEDOT:PSS with a smaller n, a smaller J_s and a higher V_{bi}.

The internal resistance (R) and capacitance (C) of hybrid solar cells are investigated using an EIS method at a bias voltage of 0.5 V. the Nyquist plots of hybrid solar cells are presented in Fig. 7a. Additionally, the proper equivalent circuit including the internal resistance and capacitance are proposed to appraise the interface quality, as illustrated in Fig. 7b. The reference device displays two semicircles of impedance spectroscopy from two major interfaces (Al/Si and Si/PEDOT:PSS), where the charge transfer and accumulation occurs, with responding frequency at 100-2×10^3 Hz and 2×10^3-1×10^6 Hz. These two *RC* elements are related to these two tandem interfaces, analysed by the equivalent circuit model of "w/o PFN" in Fig. 7b. The resistance R_{pn} and $R_{Al/Si}$ are estimated to be 1.95×10^4 Ω and 4525 Ω, respectively. Additionally, the capacitance C_{PN} and $C_{Al/Si}$ values are 1.24×10^{-9} F and 7.03×10^{-8} F, respectively. Since the rear side of wafer is more rough than the polished side, there are more surface defects to trap the charges to accumulate at Al/Si interface to present a larger capacitance. Furthermore, the minority carrier lifetime (τ_n) at the related interfaces of hybrid solar cells could be obtained from the relationship between internal resistance and capacitance, as follows:[32]

$$\tau_n = RC \quad (7)$$

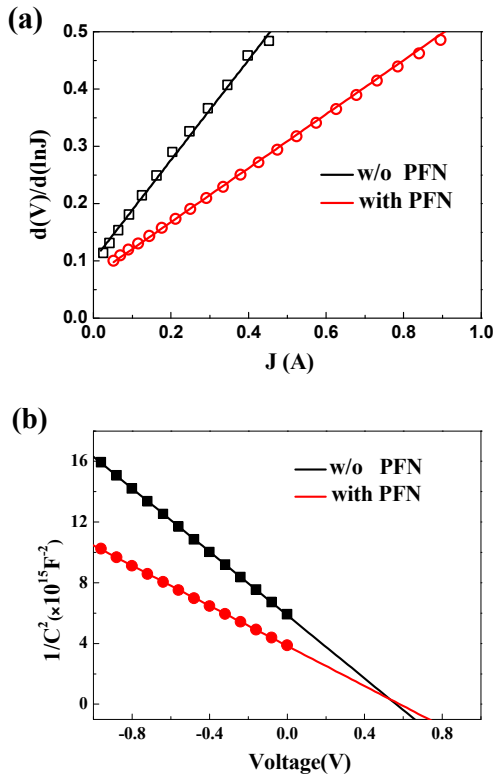

Fig. 6 (a) Plots of d(*V*)/d(ln*J*) vs. *J* (b) Capacitance *vs.* voltages curves of Si/PEDOT:PSS hybrid solar cells based on the rear electrodes with and without a PFN interfacial layer in the dark condition.

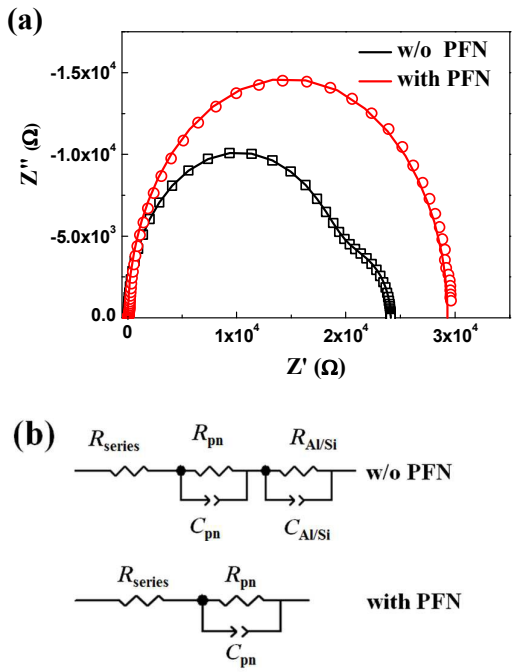

Fig. 7 (a) Experimental impedance spectra (Nyquist plots) of hybrid solar cells based on the different rear electrodes with and without PFN modification (experimental data are represented by dots and fitting data according to the relevant models are represented by lines), (b) The simplified equivalent circuit model for the spectra fitting (R_{series}: series resistance of external circuit, $R_{Si/Al}$/$C_{Si/Al}$: charge transfer resistance and capacitance at Si/Al, R_{pn}/C_{pn}: charge transfer resistance and capacitance at Si/PEDOT:PSS).

Thus, the minority carrier lifetimes at Si/PEDOT:PSS and Al/Si interfaces are 24.20 μs and 318 μs, respectively. However, the Nyquist plot of PFN device only has one semicircle, with a R_{PN} of 2.95×10^4 Ω and a C_{pn} of 2.04×10^{-8} F, which the responding frequency is at $1\text{-}1\times10^6$ Hz. The Ohmic contact received from PFN modification, eliminates the surface charge accumulation at the rear electrode for *RC* element respond. The C_{PN} value of PFN device is enhanced around 10 times than that of reference device. Moreover, the interface impedance larger, minority carrier recombination is retarded more remarkably.[33] The τ_n value of PFN device is 601 μs, 25 times larger than that of reference device, indicating the drastic reduction of charge recombination at the Si/PEDOT:PSS heterojunction.

As the discussion of electric properties previously, the conjugated polymer PFN reduces the Al WF to improve the contact quality of rear electrode. This interface modification not only offsets the negative influence of Schottky barrier at Al/Si interface for a larger J_{sc} but also enhances the total barrier height of built-in electric field of hybrid solar cell for a higher V_{oc}, leading to a better heterojunction quality. These *J-V*, *C-V* and EIS measurements verified that the PFN interlayer not only improves the electron collection efficiency of hybrid solar cell, but also suppresses the charge recombination at Si/PEDOT:PSS interfaces, receiving an excellent photovoltaic performance.

4. Conclusion

In summary, we developed a simple method to improve the rear contact from a Schottky contact to an Ohmic contact for higher photovoltaic performance. The interlayer of PFN polymer is inserted in between Al and Si for a dramatic WF reduction of Al electrode and an excellent PCE of 13.35% is received, as well as the improved V_{oc}, J_{sc} and *FF*. In addition to the light performance, the superior dark performance is also observed. These superior properties are ascribed to the formation of the rear Ohmic contact and the enhanced total built-in electric field as a result of band bending, which are extensively studied experimentally. The EIS measurement also indicates that the PFN device presents significantly enhanced minority carrier lifetime at Si/PEDOT:PSS interface. This soluble, simple and low temperature fabrication process for developing high efficiency hybrid solar cells represents a promising way for low cost photovoltaics.

Acknowledgements

This work was financially supported by Zhejiang Provincial Natural Science Foundation of China (Grant No. LR16F040002), Thousand Talent Program for Young Outstanding Scientists of People's Republic China, the Instrument Developing Project of the Chinese Academy of Sciences (Grant No. yz201328), the

National Natural Science Foundation of China (Grant No. 21403262), International S&T Cooperation Program of Ningbo (Grant No. 2015D10021), and the Natural Science Foundation of Ningbo (Grant No. 2014A610041).

Notes and references

1. M. Wright and A. Uddin, *Sol. Energy Mater. Sol. Cells*, 2012, **107**, 87-111.
2. J. P. Thomas and K. T. Leung, *Adv. Funct. Mater.*, 2014, **24**, 4978-4985.
3. Q. Liu, R. Ishikawa, S. Funada, T. Ohki, K. Ueno and H. Shirai, *Adv. Energy Mater.*, 2015, **5**, 1614-6832.
4. Y. Zhang, W. Cui, Y. Zhu, F. Zu, L. Liao, S. T. Lee and B. Sun, *Energy Environ. Sci.*, 2015, **8**, 297-302.
5. T. G. Chen, B. Y. Huang, E. C. Chen, P. C. Yu and H. F. Meng, *Appl. Phys. Lett.*, 2012, **101**, 033301-033306.
6. Q. M. Liu, M. Ono, Z. G. Tang, R. Ishikawa, K. Ueno and H. Shirai, *Appl. Phys. Lett.*, 2012, **100**, 183901-183905.
7. L. He, C. Jiang, H. Wang, D. Lai and Rusli, *Appl. Phys. Lett.*, 2012, **100**, 73503-73507.
8. H. J. Syu, S. C. Shiu and C. F. Lin, *Sol. Energy Mater. Sol. Cells*, 2012, **98**, 267-272.
9. Y. W. Zhu, T. Song, F. T. Zhang, S. T. Lee and B. Q. Sun, *Appl. Phys. Lett.*, 2013, **102**, 113504-113508.
10. J. J. P. Valeton, K. Hermans, C. W. M. Bastiaansen, D. J. Broer, J. Perelaer, U. S. Schubert, G. P. Crawford and P. J. Smith, *J. Mater. Chem.*, 2010, **20**, 543-546.
11. Z. C. He, C. M. Zhong, S. J. Su, M. Xu, H. B. Wu and Y. Cao, *Nat. Photonics*, 2012, **6**, 591-595.
12. W. D. Xu, X. W. Zhang, Q. Hu, L. Zhao, X. Y. Teng, W. Y. Lai, R. D. Xia, J. Nelson, W. Huang and D. D. C. Bradley, *Org. Electron.*, 2014, **15**, 1244-1253.
13. H. Ma, H.-L. Yip, F. Huang and A. K. Y. Jen, *Adv. Funct. Mater.*, 2010, **20**, 1371-1388.
14. X. Wang, T. Ishwara, W. Gong, M. C. Quiles, J. Nelson and D. D. C. Bradley, *Adv. Funct. Mater.*, 2012, **22**, 1454-1460.
15. Z. Zhang, X. Lu, Q. Fan, W. Hu and W. Huang, *Polym. Chem.*, 2011, **2**, 2369-2377.
16. F. Huang, Y. H. Niu, Y. Zhang, J. W. Ka, M. S. Liu and A. K. Y. Jen, *Adv. Mater.*, 2007, **19**, 2010-2014.
17. F. Huang, H. Wu, D. Wang, W. Yang and Y. Cao, *Chem. Mater.*, 2004, **16**, 708-716.
18. A. Y. C. Yu, *Solid-State Electron.*, 1970, **13**, 239-247.
19. P. L. Janega, J. McCaffrey and D. Landheer, *Appl. Phys. Lett.*, 1989, **55**, 1415-1417.
20. L. Kronik and Y. Shapira, *Surf. Sci.e Rep.*, 1999, **37**, 1-206.
21. J. He, P. Gao, M. Liao, X. Yang, Z. Ying, S. Zhou, J. Ye and Y. Cui, *ACS Nano*, 2015, **9**, 6522-6531.
22. Y. Zhou, C. Fuentes-Hernandez, J. Shim, J. Meyer, A. J. Giordano, H. Li, P. Winget, T. Papadopoulos, H. Cheun, J. Kim, M. Fenoll, A. Dindar, W. Haske, E. Najafabadi, T. M. Khan, H. Sojoudi, S. Barlow, S. Graham, J.-L. Brédas, S. R. Marder, A. Kahn and B. Kippelen, *Science*, 2012, **336**, 327-332.
23. R. Labie, T. Bearda, O. El Daif, B. O'Sullivan, K. Baert and I. Gordon, *J. Appl. Phys.*, 2014, **115**, 8.
24. K. Zhang, C. Zhong, S. Liu, C. Mu, Z. Li, H. Yan, F. Huang and Y. Cao, *ACS Appl. Mater. Interfaces*, 2014, **6**, 10429-10435.
25. D. C. Northrop and D. C. Puddy, *Nucl. Instrum. Meth.*, 1971, **94**, 557-559.
26. K. Zhang, C. M. Zhong, S. J. Liu, A. H. Liang, S. Dong and F. Huang, *J. Mater. Chem. C*, 2014, **2**, 3270-3277.
27. G. Dingemans and E. Kessels, *J. Vac. Sci. Technol. A*, 2012, **30**, 40802-40829.
28. S. Zhong, R. Wang, H. Y. Mao, Z. C. He, H. B. Wu, W. Chen and Y. Cao, *J. Appl. Phys.*, 2013, **114**, 7.
29. A. Metz, D. Adler, S. Bagus, H. Blanke, M. Bothar, E. Brouwer, S. Dauwe, K. Dressler, R. Droessler, T. Droste, M. Fiedler, Y. Gassenbauer, T. Grahl, N. Hermert, W. Kuzminski, A. Lachowicz, T. Lauinger, N. Lenck, M. Manole, M. Martini, R. Messmer, C. Meyer, J. Moschner, K. Ramspeck, P. Roth, R. Schönfelder, B. Schum, J. Sticksel, K. Vaas, M. Volk and K. Wangemann, *Sol. Energy Mater. Sol. Cells*, 2014, **120,** 417-425.
30. S. K. Cheung and N. W. Cheung, *Appl. Phys. Lett.*, 1986, **49**, 85-87.
31. F. Fabregat-Santiago, G. Garcia-Belmonte, I. M. Sero and J. Bisquert, *Phys. Chem. Chem. Phys.*, 2011, **13**, 9083-9118.
32. J. Sheng, L. Hu, S. Xu, W. Liu, L. e. Mo, H. Tian and S. Dai, *J. Mater. Chem.*, 2011, **21**, 5457-5463.
33. M. Cai, V. T. Tiong, T. Hreid, J. Bell and H. Wang, *J. Mater. Chem. A*, 2015, **3**, 2784-2793.

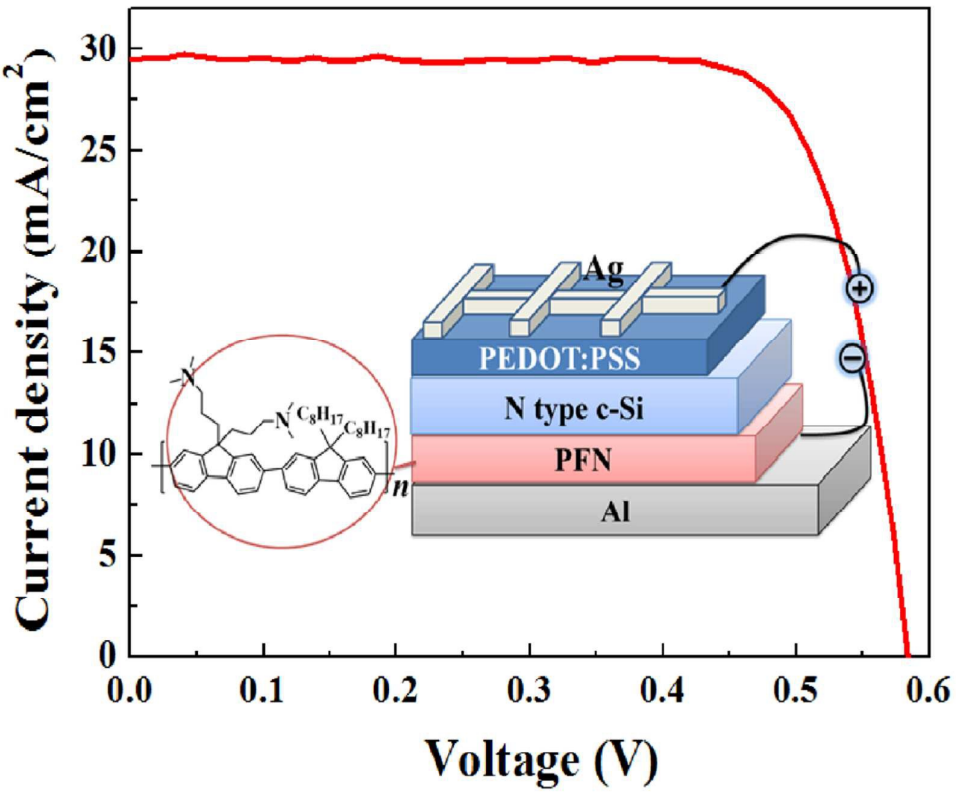

Poly[(9,9-bis(3'-(N, N-diethylamino)propyl)-2,7-fluorene)-alt-2,7-(9,9-dioctylfluorene)] (PFN), is introduced to the Al/n-Si interface to modify the contact properties, resulting in a reduced work function of Al electrode and thus a good Ohmic contact. An excellent photovoltaic efficiency of 13.35% has been achieved in a planar device with a PFN layer.